Quarterly Report for

# October - December 2001

# Stanford Geothermal Program

DE-FG07-99ID13763

# Table of Contents

# 1. STEAM-WATER RELATIVE PERMEABILITY IN FRACTURES

This project is being conducted by Research Assistants Chih-Ying Chen and Gracel Diomampo, Research Associate Kewen Li and Prof. Roland Horne. The goal is to gain better understanding of steam-water flow and mass transport through fractured media and determine the behavior of relative permeability in fractures. According to the preliminary results, the behavior of steam-water flow is different from that of air-water.

## 1.1 THEORETICAL BACKGROUND

Multiphase flow is an important behavior of geothermal reservoirs which are complex systems of porous and fractured media. Complete understanding of geothermal fluid flow requires knowledge of flow in both media. Normally, fractures are the main conduits for fluid transport in geothermal reservoirs. In geothermal reservoirs, the fluids, steam and water, are both derived from the same substance but in different phases. The phase change during steam-water flow is a physical phenomenon that does not occur in the multiphase flow of distinct fluids such as air and water, hence the multiphase flow properties are likely to differ. At present, the governing flow mechanism for boiling multiphase flow in fractures is still undetermined. There are two approaches commonly used to model multiphase flow in fractures, the porous medium approach and the equivalent homogeneous single-phase approach.

The porous medium approach treats fractures as connected two-dimensional porous media. In this model, a pore space occupied by one phase is not available for flow for the other phase. A phase can move from one position to another only upon establishing a continuous flow path for itself. As in porous media, the competition for pore occupancy is described by relative permeability and governed by Darcy's law. Darcy's law for single-phase liquid system is:

$$q_l = \frac{k_{abs}(p_i - p_o)}{\mu_l L} \tag{1.1}$$

where subscript $l$ stands for the liquid phase, $i$ for inlet and $o$ for outlet; $\mu$, $p$, $L$, $q$, $k_{abs}$ are the viscosity, pressure, fracture length, Darcy flow velocity and absolute permeability respectively. The Darcy flow velocity is equal to

$$q = \frac{Q}{bw} \tag{1.2}$$

with $Q$ as the volumetric flow rate, $b$ the fracture aperture and $w$ as the fracture width. Absolute permeability of the fracture is a function only of the fracture aperture (Witherspoon et al., 1980) as described in the cubic law

$$k_{abs} = \frac{b^2}{12} \tag{1.3}$$

For liquid phase in two-phase flow, Eqn. (1.1) becomes

$$q_l = \frac{k_{abs}k_{rl}(p_i - p_o)}{\mu_l L} \tag{1.4}$$

where $k_{rl}$ is the relative permeability of the liquid phase.

Similarly, Darcy's law derived for single-phase isothermal gas flow in porous media (Scheidegger, 1974) is

$$q_g = \frac{k_{abs}(p_i^2 - p_o^2)}{2\mu_g L p_o} \tag{1.5}$$

with the subscript *g* pertaining to the gas phase.

In two-phase flow, Eqn. (1.5) becomes

$$q_g = \frac{k_{abs}k_{rg}(p_i^2 - p_o^2)}{2\mu_g L p_o} \tag{1.6}$$

with $k_{rg}$ as the gas relative permeability. The sum of the $k_{rl}$ and $k_{rg}$ indicates the extent of phase interference. A sum of relative permeabilities equal to one means the absence of phase interference. Physically this implies each phase flows in its own path without impeding the flow of the other. The lower is the sum of the relative permeabilities from unity the greater is the phase interference.

Relative permeability functions are usually taken to be dependent on phase saturation. The two most commonly used expressions for relative permeability for homogeneous porous media are the X-curve and Corey curve (Corey, 1954). The X-curve takes relative permeability as linear function of saturation

$$k_{rl} = S_l \tag{1.7}$$

$$k_{rg} = S_g \tag{1.8}$$

where $S_l$ and $S_g$ are the liquid and gas saturation respectively. The Corey curve relates relative permeability to the irreducible or residual liquid and gas saturation, $S_{rl}$ and $S_{rg}$

$$k_{rl} = S^{*4} \tag{1.9}$$

$$k_{rg} = (1 - S^*)^2(1 - S^{*2}) \tag{1.10}$$

$$S^* = (S_l - S_{rl})/(1 - S_{rl} - S_{rg}) \tag{1.11}$$

The equivalent homogeneous single-phase approach treats flow through fracture as a limiting case of flow through pipes. In this model, phase velocities in a fracture are equal and capillary forces are negligible. A continuous flow path is not required for movement of each phase. A phase can be carried along by one phase as bubbles, slug or other complex structures. As in pipes, flow can be described by the concept of friction factors and using averaged properties (Fourar et al., 1993)

$$(p_i - p_o) = \frac{\Pi f \rho_m V_m^2}{2A} \tag{1.12}$$

where $\Pi$ is the fracture perimeter, $A$ is the cross sectional area to flow, $\rho_m$ average density and $V_m$ as average flow velocity. The average density is described by

$$\rho_m = \frac{\rho_g Q_g + \rho_l Q_l}{Q_g + Q_l} \tag{1.13}$$

The average flow velocity is equal to

$$V_m = \frac{Q_g + Q_l}{A} \tag{1.14}$$

The friction factor, *f*, is derived empirically as a function of the averaged Reynolds number calculated by

$$N_{\mathrm{Re}} = \frac{2bV_m\rho_m}{\mu_m} \tag{1.15}$$

with $\mu_m$ as average viscosity

$$\mu_m = \frac{\mu_g Q_g + \mu_l Q_l}{Q_g + Q_l} \tag{1.16}$$

There are several expressions used to relate friction factor and Reynold's number. The commonly used one for flow through fracture is the generalized Blasius form (Lockhart and Martinelli, 1949):

$$f = \frac{C}{N_{\mathrm{Re}}^n} \tag{1.17}$$

with *C* and *n* as constants derived from experimental data.

According to the results from Diomampo (2001), the nitrogen-water flow through fracture is described more appropriately by using the porous medium (relative permeability) approach. However in the steam-water case, the applicability of the two models for multiphase flow through fractures is still undetermined.

## 1.2 LITERATURE REVIEW

The fluids in geothermal reservoirs, steam and water, are both derived from the same substance. However, they form different phases. The phase change during steam-water multiphase flow has made it difficult to investigate steam-water relative permeability. Even in multiphase flow without boiling, only a few published data are available for two-phase flow in fractures. Most of the studies have been done for air-water systems or for water-oil systems.

Earliest is Romm's (1966) experiment with kerosene and water through an artificial parallel-plate fracture lined with strips of polyethylene or waxed paper. Romm found a linear relationship between permeability and saturation, $S_w = k_{rw}$, $S_{nw} = k_{rnw}$ such that $k_{rw}+k_{rnw} = 1$. Fourar et al. (1993) artificially roughened glass plates with beads and flowed air-water between them. Fourar and Bories (1995) did similar experiments using smooth glass plates and clay bricks. Both studies observed flow structures like bubbles, annular and fingering bubbles comparable to flow in pipes and depicted flow in fractures to be better correlated using the equivalent homogeneous single-phase model. Pan et al. (1996) observed the identical flow structures in their experiment with oil-water system. They observed that a discontinuous phase can flow as discrete units along with the other phase. Pan et al. (1996) also found their experimental pressure drop to be better predicted by homogenous single-phase model. All of these experiments show significant phase interference at intermediate saturations.

Pruess and Tsang (1990) conducted numerical simulation of flow through rough-walled fractures. They modeled fractures as two-dimensional porous media with apertures varying with position. Their study showed the sum of the relative permeabilities to be less than 1, the residual saturation of the nonwetting phase to be large and phase interference to be greatly dependent on the presence or absence of spatial correlation of aperture in the direction of flow. Persoff et al. (1991) did experiments on gas and water flow through rough-walled fractures using transparent casts of natural fractured rocks. The experiment showed strong phase interference similar to the flow in porous media. The relative permeability data of Persoff (1991) and Persoff and Pruess (1995) for flow through rough-walled fractures were compared in Horne et al (2000) against commonly used relative permeability relations for porous media, the X-curve and Corey curve, as shown in Figure 1.1. Diomampo (2001) performed experiments of nitrogen and water flow through both smooth- and rough-walled artificial fractures, leading to results that are also included in Figure 1.1.

In the experiments of both Persoff (1991) and Persoff and Pruess (1995), flow of a phase is characterized by having a localized continuous flow path that is undergoing blocking and unblocking by the other phase. Recent parallel plate experiments by Su et al. (1999) illustrate the same flow mechanism of intermittent localized fluid flow. Kneafsy and Pruess (1998) observed similar intermittent flow in their experiments with pentane through various parallel plate models made from glass, sandblasted glass or transparent fracture replicas. Diomampo (2001) also found the intermittent phase change phenomenon in her experiments. Furthermore, the results from her experimental data conform mostly to the Corey type of curve (Figure 1.1). This suggests that flow through fractures can be analyzed by treating it as a limiting case of porous media flow and by using the relative permeability approach. These observations are contrary to the findings of Fourar et al (1993), Fourar and Bories (1995), and Pan et al. (1996).

Presently, the mechanism of flow and the characteristic behavior of relative permeability in fractures are still undetermined. Issues such as whether a discontinuous phase can travel as discrete units carried along by another phase or will be trapped as residual saturation as in porous medium are unresolved. The question of phase interference i.e. is the relative permeability curve against saturation an X-curve, Corey or some other function is still unanswered. The main objective of this study was to contribute to the resolution of these issues. Experiments on flow through smooth-walled fractures without boiling have been conducted by Diomampo (2001). She has established a reliable methodology for flow characterization and permeability calculation for nitrogen-water flow. Currently, steam-water system experiments are in progress.

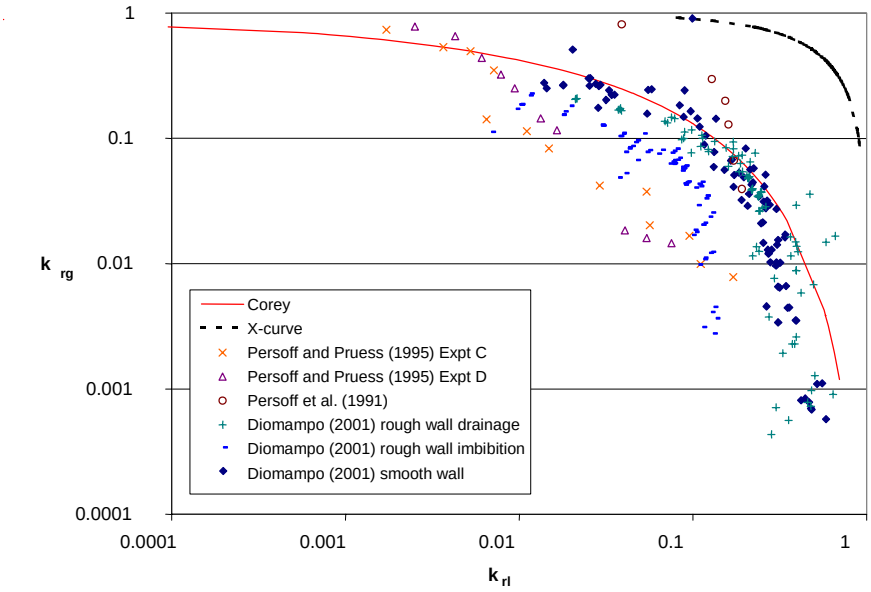


*Figure 1.1: Compendium of previous measurements of air-water relative permeabilities in fractures (from Diomampo, 2001).*

## 1.3 EXPERIMENTAL METHODOLOGY

The steam-water flow experiment is more complex the than air-water experiment conducted previously by Gracel Diomampo (2001). The steam-water flow experiment has to be performed at high temperature. The whole experiment system is shown in Figure 1.2, which shows the deaerated water supply, the fracture apparatus (inside the air bath), data acquisition system, and digital image recording.

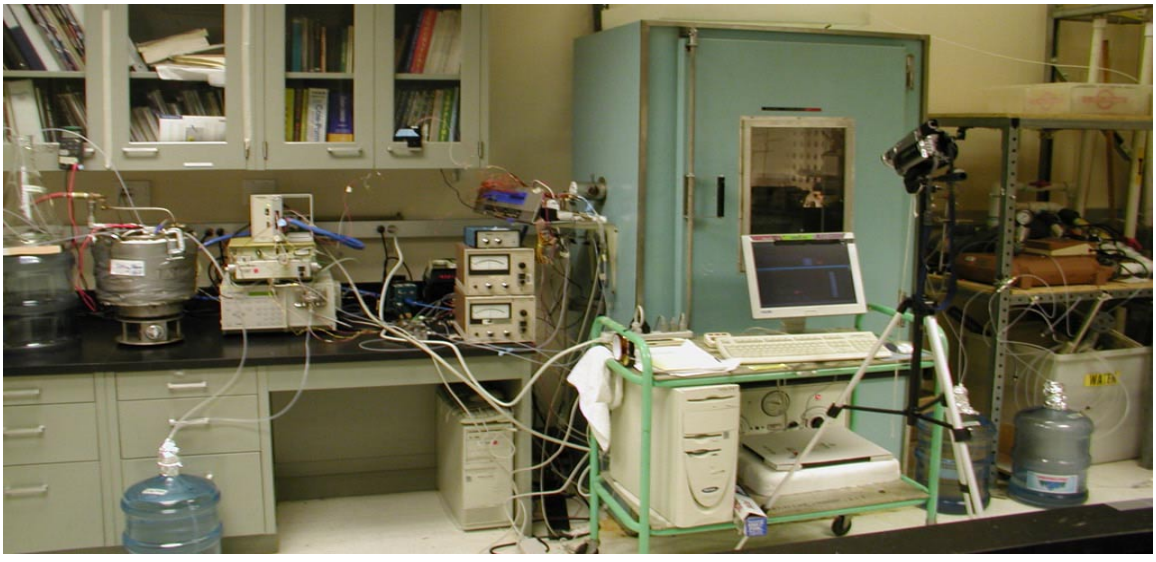

*Figure 1.2: Picture of steam-water flow through fracture apparatus.*

## Fracture Apparatus Description

The fracture is created by a smooth glass plate on top of an aluminum plate. The whole apparatus is confined by a metal frame bolted to the bottom plate. This was done to improve the seal and to prevent deformation of the glass due to system pressure. The metal frame has several windows and a mirror attached to it for flow visualization. (See Figure 1.3 and Figure 1.4.)

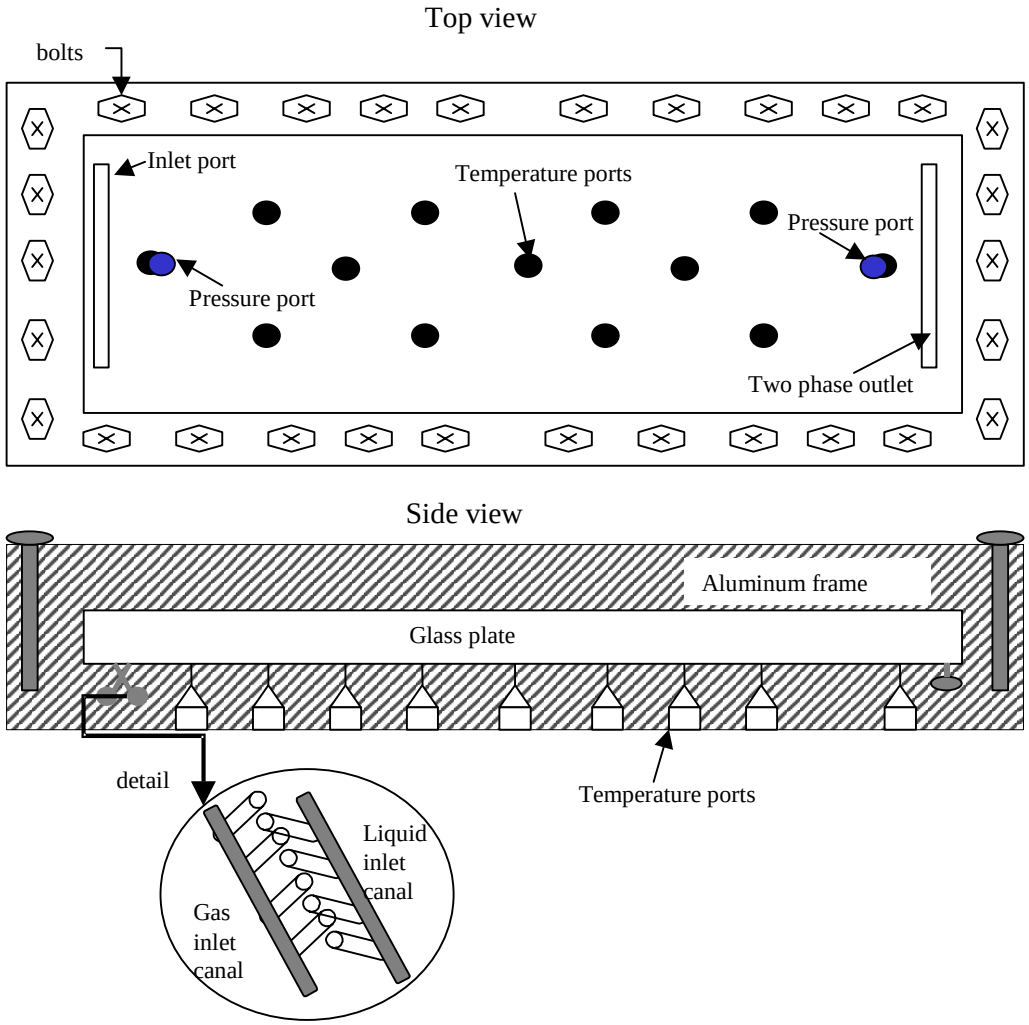


*Figure 1.3: Schematic diagram of fracture apparatus.*

*Figure 1.4: Picture of fracture apparatus.*

An O-ring (Viton 1/8" thick #2-272) was placed in between the glass and aluminum plate as a seal (see orange color lining in Figure 1.4). Placing this O-ring in the channel was not sufficient to provide a good seal because the channel was custom made in width and length. Thinly cut rubber sheets were placed at the outer boundary to push the O-ring to the sides of the aluminum plate. These provided an excellent seal when compressed with the glass and metal frame. Since the O-ring is cylindrical in shape and the aluminum plate is rectangular; there will be a narrow channel in between the O-ring and the plate when squeezed together. A thin lining of copper based adhesive (Permatex Ultra Copper) was applied to fill this channel. It is important to eliminate this channel for it serves as an easy conduit for the fluid to pass through instead of the fracture.

The phases enter the fracture through two separate canals. Each canal has several ports drilled in a way that they align on the surface (See Figure 1.3). The surface of the fracture apparatus was designed such that there is an available 12 inch by 4 inch space for flow. Through out this flow area, tiny temperature ports the size of needles were drilled. Needle-size ports were drilled so as to minimize surface discontinuity. A pressure port was drilled at each end of the flow path. The two-phase fluid exits through a single outlet.

**Fractional Flow Ratio Detector**

One of the biggest challenges of steam-water flow experiment is to measure the steam and water flow rates, since there is phase transition occurring when steam and water flow through the fracture. Therefore using flow meters to measure the rate of each phase become inappropriate, because it is always impossible to separate steam from water without any mass loss or gain. To overcome this situation, an in-situ fractional flow ratio detector (FFRD) was designed and constructed as shown in Figure 1.5. The principal of the FFRD is that different phases will have different refractive indices. A phototransistor was installed inside the FFRD, producing different voltages when sensing different strengths of light. The water phase produces a higher voltage when flowing through the FFRD. An example of the FFRD response signal during testing is shown in Figure 1.6.

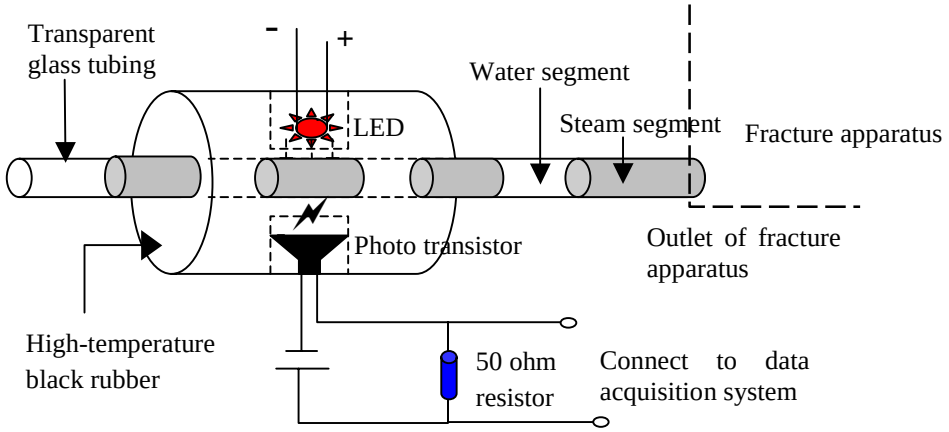


*Figure 1.5: Schematic of fractional flow ratio detector (FFRD).*

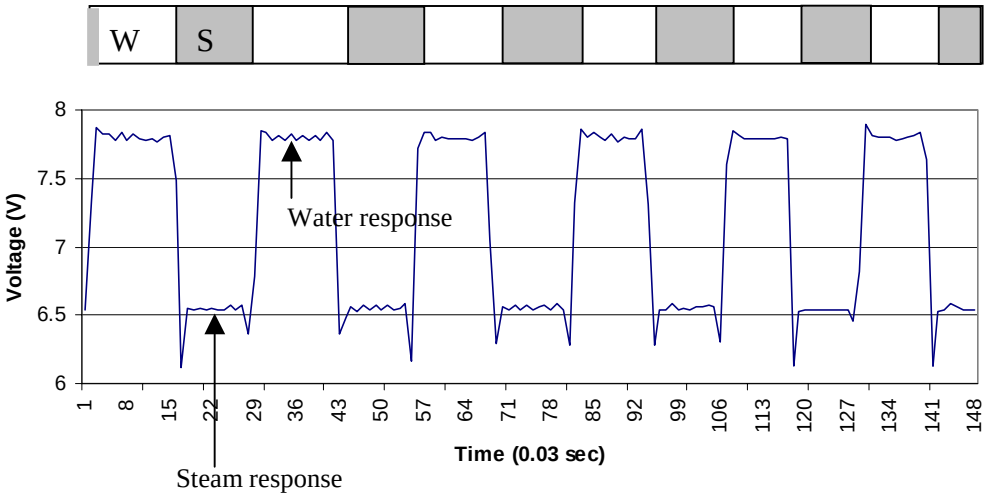


*Figure 1.6: The signal of steam and water detected from fractional flow ratio detector.*

Once the steam and water responses are obtained from the FFRD, the statistical histogram is plotted and the steam and water phase flow ratios are obtained by determining the threshold of the histogram. This is shown in Figure 1.7.

The calibration test of FFRD has been completed as shown in Figure 1.8. As can be seen from Figure 1.8, at both high and low water flow rates the FFRD shows high accuracy in measuring fractional flow at different nitrogen flow rates. Even when the nitrogen flow rate is much higher than the water flow rate, the FFRD can recognize the fractional flow ratio over a period of several seconds. Therefore, the FFRD technology should be appropriate to calculate steam and water outlet flow rates.

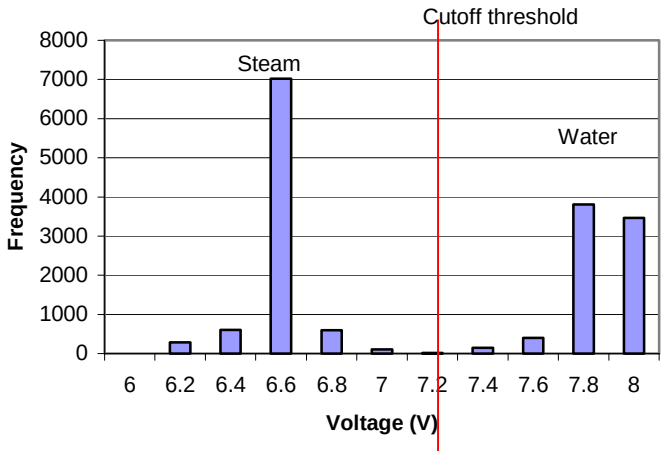


*Figure 1.7: The histogram obtained from Figure 1.6.*

*Table 1.1: The analysis results of steam and water fractional flow ratios from Figure 1.7.*

| *Bin* | *Frequency* | Discrimination |
|---|---|---|
| 6.2 | 287 | Steam |
| 6.4 | 603 | Steam |
| 6.6 | 7021 | Steam |
| 6.8 | 600 | Steam |
| 7 | 110 | Steam |
| 7.2 | 20 | Threshold |
| 7.4 | 146 | Water |
| 7.6 | 400 | Water |
| 7.8 | 3810 | Water |
| 8 | 3462 | Water |
| More | 0 | |

| | |
|---|---|
| Steam Total | 8631 |
| Water Total | 7828 |
| Grand total | 16459 |

| Fractional flow | |
|---|---|
| Steam | 0.5243939 |
| Water | 0.4756061 |

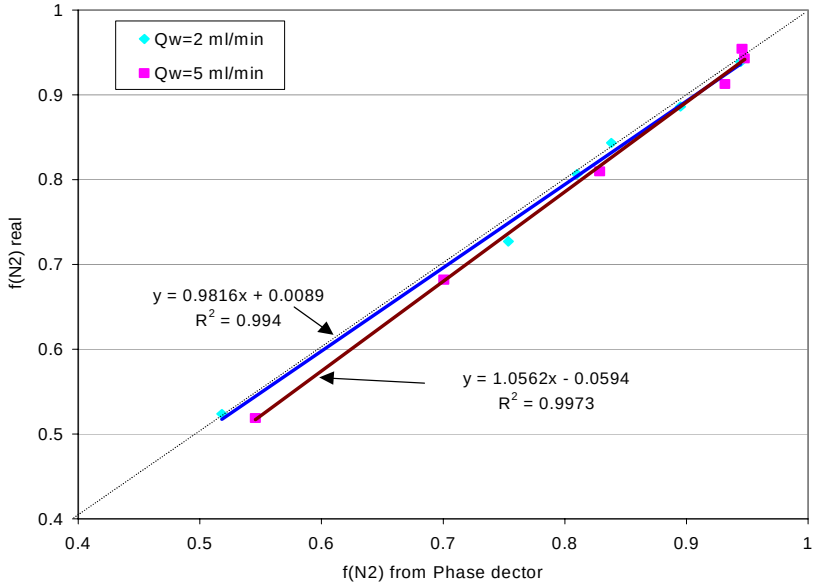


*Figure 1.8: The calibration of FFRD in nitrogen-water flow.*

## Control and Measurement Techniques

There are two methods available to produce steam-water flow inside the fracture. One method is by injecting steam and water separately into the apparatus. The steam would be produced using a steam generator inside the air bath to boil steam from deaerated water. The other method is by injecting only deaerated water into the apparatus, after which the steam phase is produced by adjusting either pressure or temperature in the fracture. Since the steam quality from the steam generator is hard to control and there is a significant phase transformation at the moment when the injected steam and water meet in the inlet port, the latter method was used in this experiment.

The two factors that control the steam production are temperature and pressure. According to experience, adjusting pressure requires less equilibrium time than adjusting temperature. To facilitate pressure adjustment, a back-pressure device was connected to the outlet of the apparatus to constrain the pressure inside the fracture to a specific. For water, a meter pump (Dynamax, SD-200) controlled the rate of injection. The water used in the experiment needs to be deaerated almost completely. To reach this quality, distilled water was vacuumed using a vacuum pump for 2 hours, and then the water was boiled to achieve low dissolved gas condition. This distilled, deaerated water was used as the injection fluid. Figure 1.9 shows a schematic diagram of this configuration.

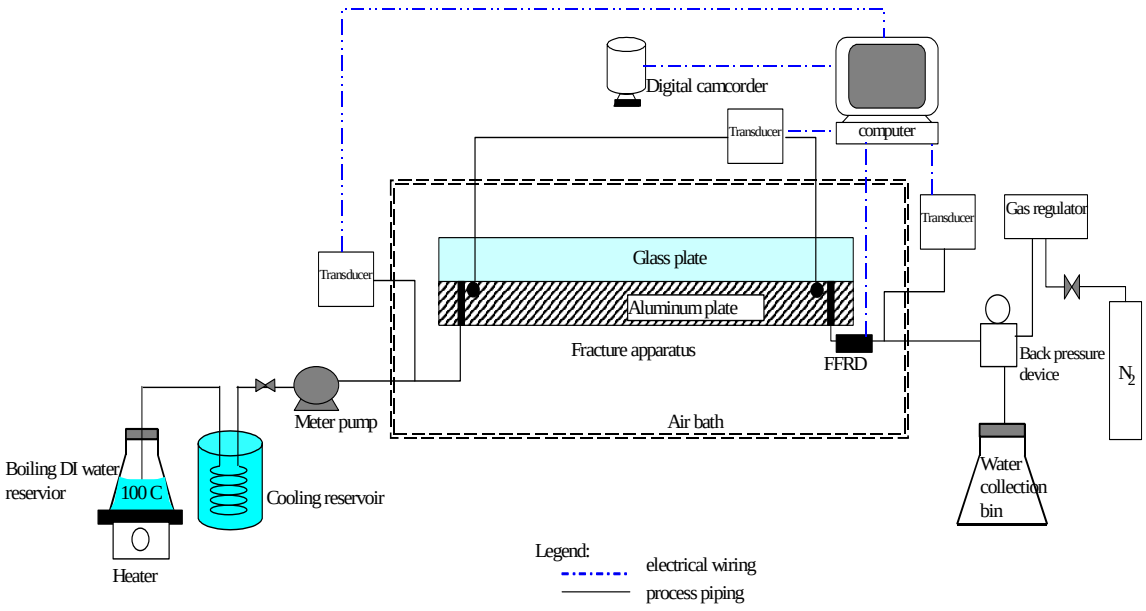


*Figure 1.9: Process flow diagram for steam-water experiment.*

Low-capacity differential transducers were used to measure the pressure drop through the fracture, water inlet pressure and the two-phase outlet pressure. The liquid differential transducer (Celesco Transducer Model CD 10D range 0-5psi) was attached to both pressure ports inside the fracture to measure the pressure drop through the fracture. Another transducer (Celesco Transducer Model CD 10D range 0-25psi) was attached to

the water inlet. The third transducer (Celesco Transducer Model CD 10D range 0-25psi) was attached to the two-phase outlet of the fracture apparatus. These transducers send electrical signals to the SCXI-1000 data acquisition device which was monitored using the LabView® programmable virtual instrument software.

For steam and water flow rates measurement, the fractional flow ratio detector (FFRD) was used to measure the outlet steam and water fractional flow ratio, $f_s$ and $f_w$.

$$f_s = \frac{Q_{s,out}}{Q_{out}} \tag{1.18}$$

$$f_w = \frac{Q_{w,out}}{Qout} \tag{1.19}$$

where $Q_{s,out}$ is the output steam flow rate, $Q_{w,out}$ is the output water flow rate, and $Q_{out}$ is the output total flow rate. Once $f_s$ and $f_w$ are obtained, it is easy to evaluate $Q_{s,out}$ and $Q_{w,out}$ if a steady state condition is reached. In order to catch the fast and unsteady steam and water segment in the outlet tubing, The FFRD was connected to the SCXI-1000 data acquisition device, which has 33Hz maximum sampling frequency.

According to the nitrogen-water experiments by Diomampo (2001) and others, these fracture flow experiments are unsteady state by nature. There are significant pressure fluctuations accompanied by saturation changes and the gas or water flow rate varies. Due to this behavior, the data acquisition task requires gathering frequent values of instantaneous pressure, flow rate and saturation. Instantaneous gathering of data was accomplished by the use of a digital video camcorder. Video shots were taken of the pressure, time and saturation data displayed all at the same time. Pressure data and related time were displayed by the LCD monitor connected to the computer which also ran the data acquisition system. The saturation was computed from the image of the whole flow area of the fracture. Still images were then taken from the recorded video. The data gathered from the video was correlated with the Labview data through the time read from the LCD monitor. Figure 1.10 shows a typical video image taken from the experiments. See also Figure 1.9.

**Saturation Measurement**

From the still image shown in Figure 1.10, saturation was computed by measuring the area that each phase occupied. The photographs were processed in a Matlab program. The program first cuts the photograph to display just the image of the flow area. Using this cut image, the program does quadratic discriminant analysis to group the pixels of the picture into three groups: the water phase, steam phase and the frame. The grouping is based on color differences. Saturation is calculated as total pixels of the liquid group over the sum of the steam and liquid groups. Figure 1.11 is a comparison of the gray-scaled image produced by the program and the original cut photograph from the digital camcorder. The accuracy of the program in calculating the saturation can be related to the similarity in details of the gray scale image to the true image. From the figure, it can be said that the program has reasonable accuracy.

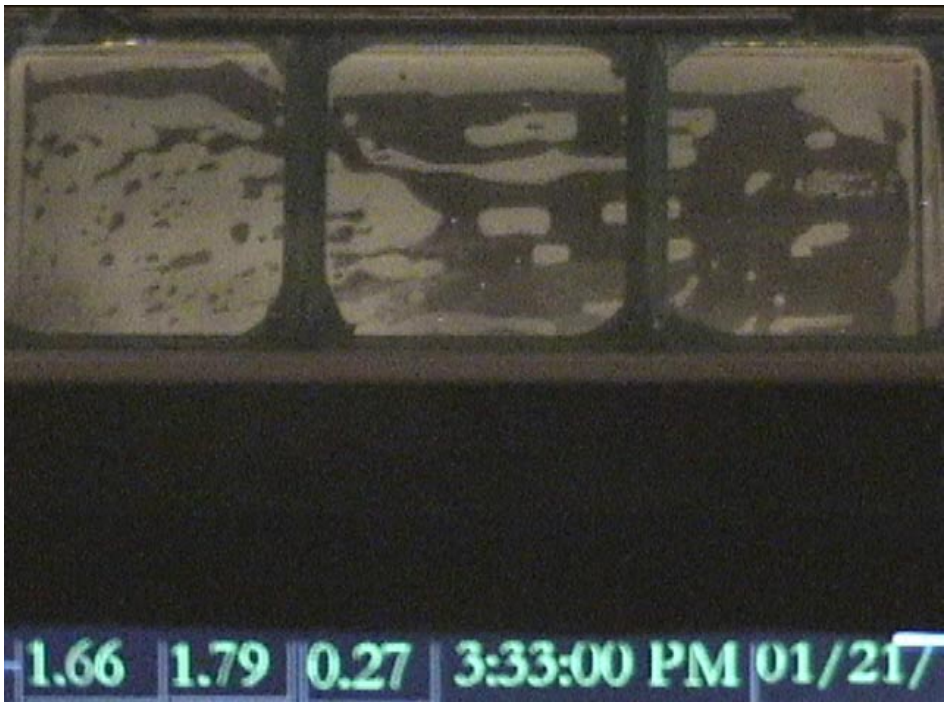


*Figure 1.10: Sample video image taken for steam-water runs.*

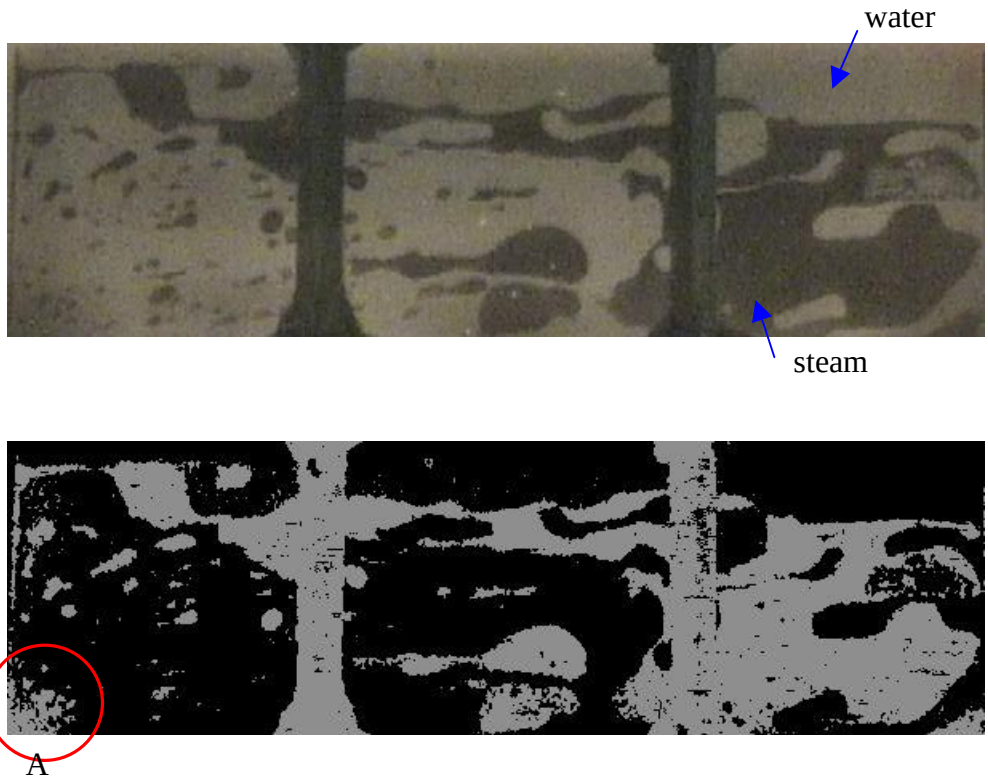


*Figure 1.11: Comparison between the true color image of the fracture flow and gray scale image from Matlab program used in measuring saturation.*

Pan et al. (1996) also used this technique for measurement of saturation. This study noted that the sources of error in this technique were the quality of the photographs and the water film adsorbed on the surfaces of the plates with the latter being of minimal effect. Good quality photographs are the ones with clear distinction between the gas and liquid phase. Good lighting is necessary so that the colors in the image come out clear. The lighting should also be positioned in a way that it does not produce shadow on the flow area. The program will mistakenly take the shadow as steam phase even if there is liquid (Zone A in Figure 1.11).

## 1.4 PRELIMINARY RESULTS AND DISCUSSION

A drainage steam-water flow through a smooth-walled fracture experiment has been conducted. Some images have been analyzed, and the corresponding saturation has been obtained satisfactorily. As observed from the video record, the steam-water flow behavior in the fracture is significantly different from the nitrogen-water flow behavior described by Diomampo (2001) in the same fracture.

Figure 1.12 shows four consecutive images taken when the water injection rate was 2 ml/min, temperature is 102$^{o}$C, and pressure was around 16.5 psia. The steam (dark part) never forms a stable path or channel, but behaves like moving metamorphic fingerings and bubbles. These physical phenomena are different from those observed by Diomampo (2001) as shown in Figure 1.13.

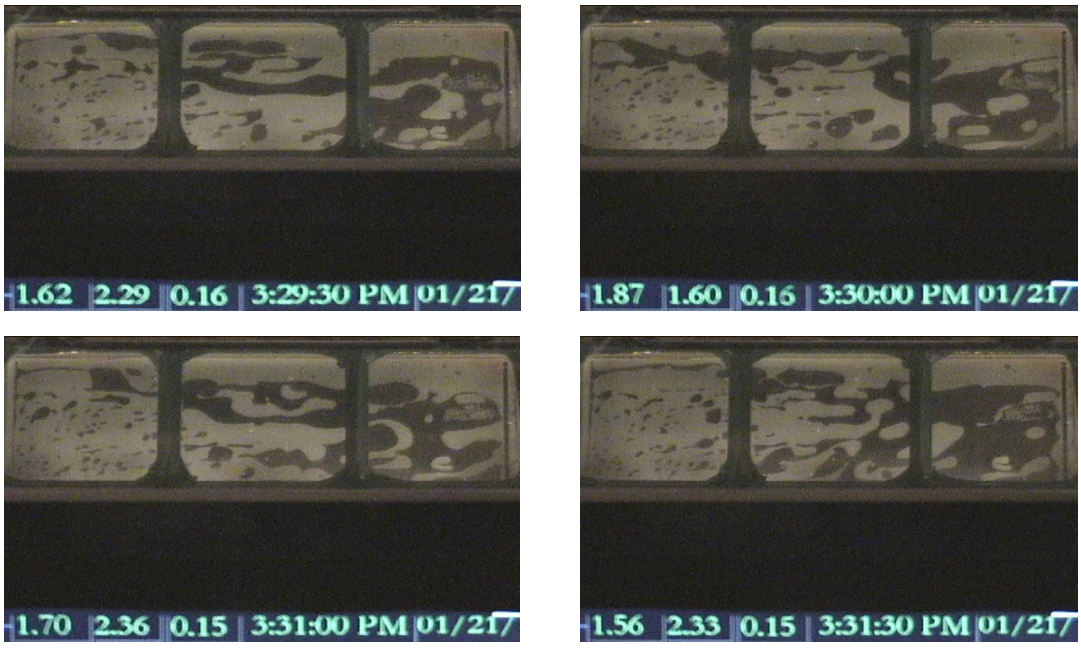


*Figure 1.12: The continuous steam-water flow behavior in smooth-walled fracture (steam phase is dark, water phase is light).*

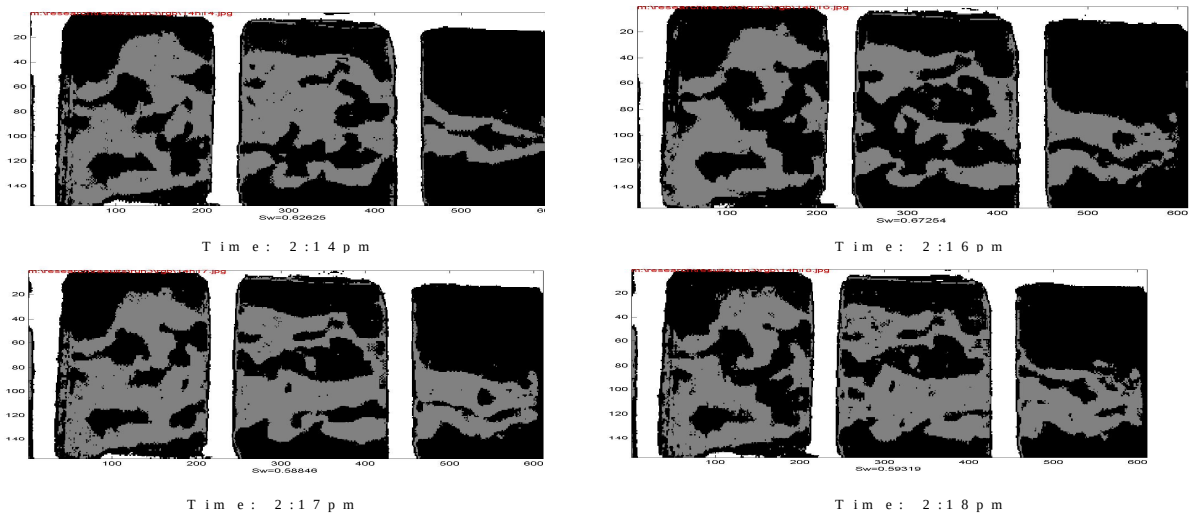


*Figure 1.13: The continuous nitrogen-water flow behavior in smooth-walled fracture. Images showing the forming and breaking of gas flow path (light part) (images from Diomampo, 2001).*

Comparing Figure 1.12 with Figure 1.13, there is less steam phase near the inlet (the left side) in steam-water flow in comparison to the nitrogen phase near the inlet in nitrogen-water flow. This is because the phase transformation from water to steam as pressure decreases in steam-water flow. Hence the farther the water flows, the more steam it produces. This will be an important factor affecting the steam-water flow behavior.

Some of the early data has been used to calculate a preliminary steam-water relative permeability curve by assuming that steady state was achieved while the image was taken and applying Equations 1.4 and 1.5. This preliminary result is shown in Figure 1.14.

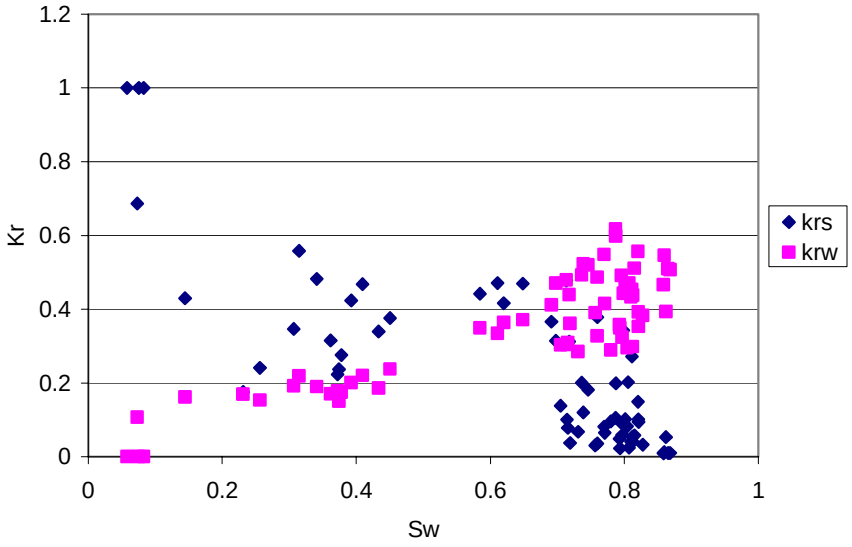


*Figure 1.14: Preliminary results for steam-water relative permeability in smooth-walled fracture.*

## 2. DECLINE ANALYSIS AT THE GEYSERS

This project is being conducted by Research Associate Kewen Li and Professor Roland Horne. The objective of this project is to develop a decline analysis method based on the theory of fluid flow instead of empiricism to predict the production performance and estimate the recoverable reserves of geothermal reservoirs.

### 2.1 SUMMARY

A decline curve analysis model was developed based on the theory of fluid flow mechanisms with relative permeability and capillary pressure included. The model reveals a linear relationship between the production rate and the reciprocal of the accumulated production. We applied the model to the production data of over 20 production wells in The Geysers geothermal field and found a linear relationship between the production rate and the reciprocal of the cumulative production for most of the wells, especially at the late period of production. This implies that we may be able to estimate the reservoir properties and the reserves. Unlike the empirical decline curve analysis methods, one of the advantages of this method is that the two constants obtained from the linear relationship have clear physical significance.

### 2.2 INTRODUCTION

Estimating reserves and predicting production performance in geothermal and petroleum reservoirs is an important but difficult task for reservoir engineers. Many papers regarding decline curve analysis methods (Chen and Teufel, 2000; Faulder, 1997; Fetkovich, 1980; Fraim and Wattenbarger, 1987; Palacio and Blasingame, 1993 and Rodriguez and Cinco-Ley, 1993) have been published in literature. However most of the existing decline curve analysis approaches are based on the empirical exponential, hyperbolic, and harmonic equations suggested by Arps (1945). Each approach has some disadvantages. For example, the exponential decline curve tends to underestimate reserves and production rates; the harmonic decline curve has a trend to overpredict the reservoir performance. This is not surprising for empirical techniques.

Previously, we developed a model to characterize the spontaneous water imbibition into gas-saturated rocks (see Li and Horne, 2001a). The model reveals a linear relationship between the imbibition (production) rate and the reciprocal of the gas recovery (cumulative production). Although this model was derived for spontaneous water imbibition, according to our derivation it is suitable for gravity drainage or other displacement processes if a piston-like saturation change is assumed. Here, we used this model to analyze the production performance of The Geysers geothermal field.

### 2.3 THEORY

The mathematical model that we developed previously to characterize the spontaneous water imbibition into gas-saturated rocks is the basis of this study. The model (Li and Horne, 2001) is expressed as follows:

$$q_w = a\frac{1}{R} - b \tag{2.1}$$

where $q_w$ is the water imbibition rate; $R$ is the recovery in terms of pore volume. $a$ and $b$ are two constants associated with capillary and gravity forces respectively. The details on deriving Eq. 2.1 and calculating $a$ and $b$ are described in Li and Horne (2001). Constant $a$ is expressed as follows:

$$a = \frac{Ak_w(S_{wf} - S_{wi})}{\mu_w L} P_c \tag{2.2}$$

where $A$ and $L$ are the cross-section area and the characteristic height of the matrix respectively, $\mu_w$ is the viscosity of water, $S_{wi}$ is the initial water saturation and $S_{wf}$ is the water saturation behind the interface of gas-water or steam-water; $k_w$ is the effective permeability of the water phase at $S_{wf}$. Similarly, $P_c$ is the capillary pressure at $S_{wf}$. Constant $b$ is expressed as follows:

$$b = \frac{Ak_w}{\mu_w}\Delta\rho g \tag{2.3}$$

where $\Delta\rho$ is the density difference between water and steam and $g$ is the gravity constant.

Eq. 2.1 could be expressed as follows in terms of cumulative steam production instead of recovery:

$$q_s = a_v\frac{1}{N_p} - b \tag{2.4}$$

where $q_s$ is the steam production rate and $N_p$ is the cumulative steam production. $a_v$ is defined as follows:

$$a_v = aV_p \tag{2.5}$$

here $V_p$ is the pore volume controlled by the production well or the reservoir.

The maximum cumulative steam production may be estimated by setting the steam production rate to be zero or an economic limit once the linear relationship between the steam production rate and the reciprocal of the cumulative steam production is obtained. Then the reserves controlled by this well can be calculated as $a_v/b$ according to Eq. 2.4.

We applied Eq. 2.5 to the production data of about 20 production wells in The Geysers geothermal field and found a linear relationship between the steam production rate and the reciprocal of the cumulative steam production for most of the wells, especially at the late period of production. The results will be discussed in the next section.

## 2.4 RESULTS

The production data from The Geysers geothermal field were used to verify the decline curve analysis method that we proposed. Figure 2.1 shows the relationship between the steam production rate and the reciprocal of the cumulative steam production from Well 1. The relationship is close to linear, so the two constants $a_v$ and $b$ can be calculated using the linear model represented by Eq. 2.4. The product of the effective permeability of the water phase and the area controlled by the production well may be evaluated according to Eq. 2.3 using the value of constant $b$. The maximum cumulative steam production $N_{pmax}$ can also be estimated once the values of the two constants $a_v$ and $b$ are available ($N_{pmax} = a_v/b$).

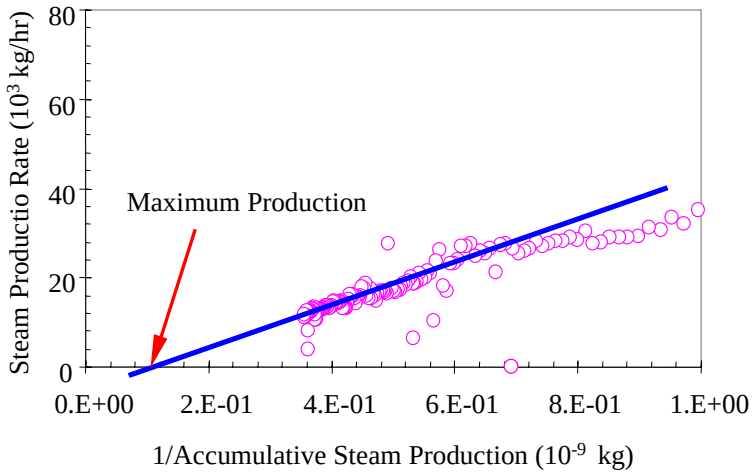


*Figure 2.1: Relationship between the steam production rate and the reciprocal of the cumulative steam production (Well 1).*

Other examples of the linear relationship between the steam production rate and the reciprocal of the cumulative steam production from different production wells are shown in Figs. 2.2 - 2.5. Each of the four production wells has a linear relationship in the late production periods. Some of the wells have similar values of $a_v$ and $b$, which implies that these wells may have similar recoverable reserves and reservoir properties. This phenomenon may be related to the region and the geology. We will investigate the coupling of the values of $a_v$ and $b$ with the geological properties in more detail.

We also used data from oil production examples to verify the approach that we have proposed here. Oil production data from Cuttler (1924) are plotted in Fig. 2.6 in terms of production rate and the reciprocal of cumulative oil production. A linear relationship was also obtained. This is not surprising, since we showed already in our previous quarterly report that Eq. 2.1 also holds in oil-water-rock systems except that the representations of the two constants $a$ and $b$ are different.

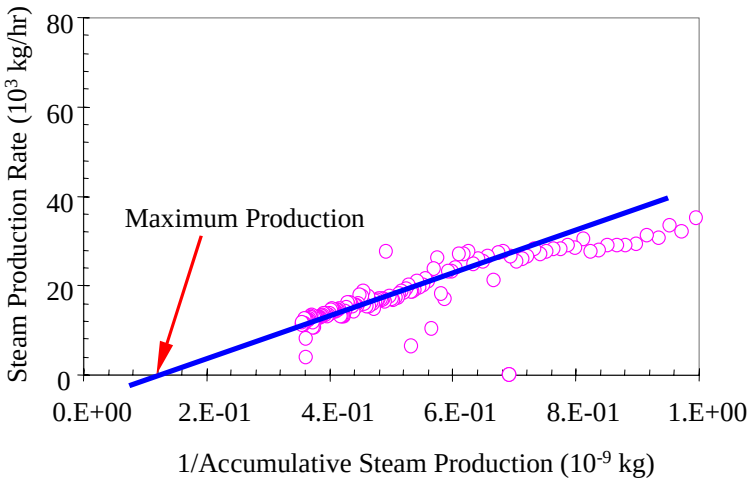


*Figure 2.2: Relationship between the steam production rate and the reciprocal of the cumulative steam production (Well 2).*

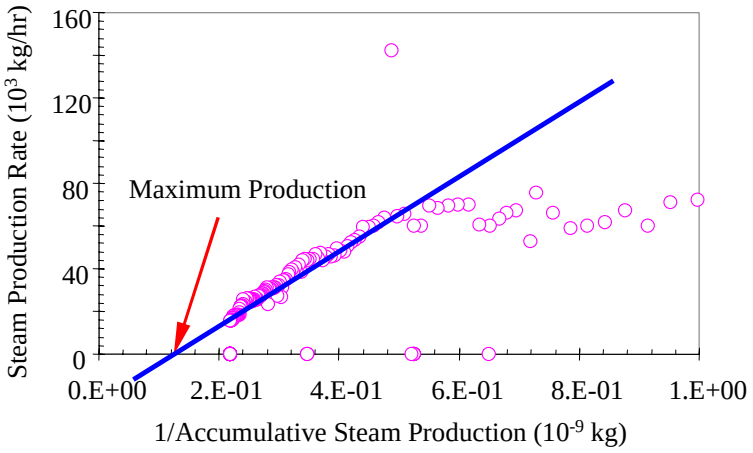


*Figure 2.3: Relationship between the steam production rate and the reciprocal of the cumulative steam production (Well 3).*

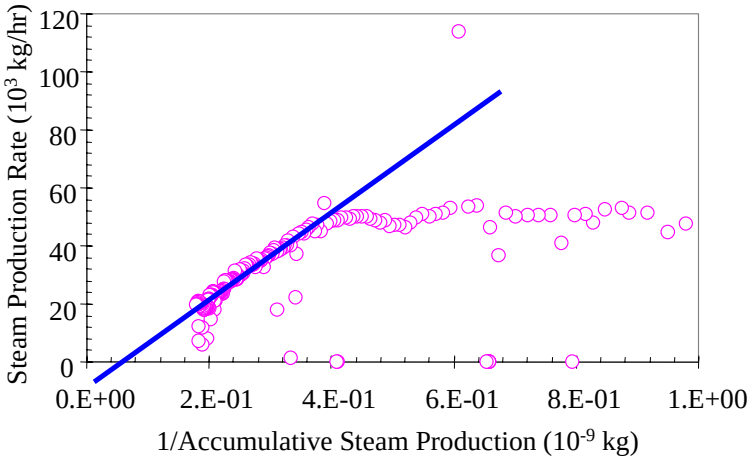


*Figure 2.4: Relationship between the steam production rate and the reciprocal of the cumulative steam production (Well 4).*

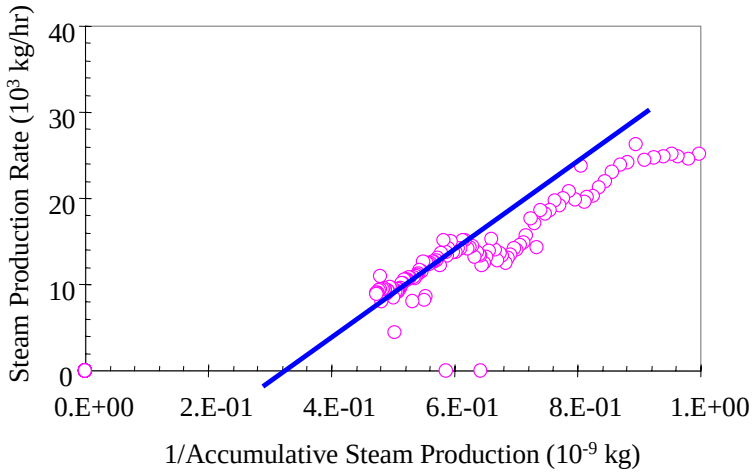


*Figure 2.5: Relationship between the steam production rate and the reciprocal of the cumulative steam production (Well 5).*

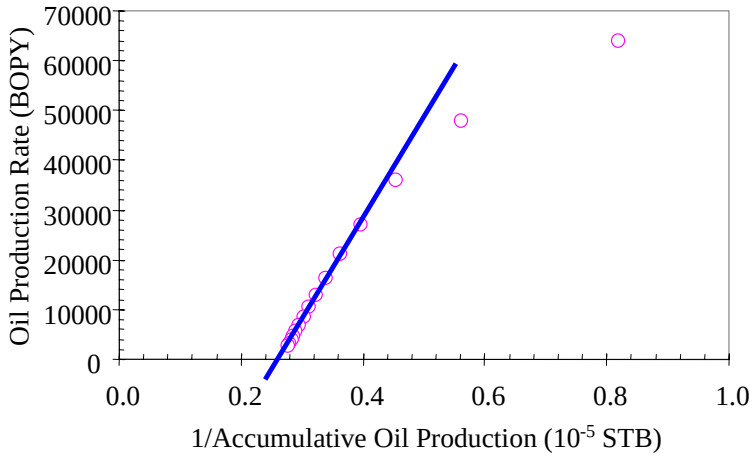


*Figure 2.6: Relationship between the oil production rate and the reciprocal of the cumulative oil production (production data from Cuttler, 1924).*

## 2.5 DISCUSSION

Eq. 2.4 was derived for a simple linear fluid flow. Due to the complexity of reservoir conditions, it may be necessary to modify Eq. 2.4 by considering heterogeneity, fracture density, compressibility, boundary conditions, radial flow, and other factors.

## 2.6 CONCLUSIONS

Based on the present study, the following conclusions may be drawn:

1. An analytical decline curve analysis model was developed based on the theory of fluid flow in porous media and was verified using the production data from both geothermal and oil reservoirs.
2. The relationship between the production rate and the reciprocal of the cumulative production is linear and may be used to estimate reservoir properties and recoverable reserves.

# 3. FRACTURED ROCK RELATIVE PERMEABILITY

This project is being conducted by Research Assistant Mark D. Habana, Research Associate Kewen Li and Prof. Roland N. Horne. The objective is to measure relative permeability relations for steam and water flow in a fractured geothermal rock. This work is an extension of current studies of steam-water flows, which have so far considered only artificially uniform porous rock. This quarter, an experiment was conducted to determine resistivity-saturation correlation for the core using two metal endplates.

## 3.1 BACKGROUND

Various works on flow through fractures showed different kinds of relative permeability behavior. Experimental studies by Persoff and Pruess (1995) resulted in curves that can not be classified either as Corey type or as linear (X-curve) type. Fourar et al. (1993) suggested that multiphase interaction in a fracture is a function of flow velocity and therefore relative permeability is not the appropriate way to describe multiphase flow in fractures.

Past experiments have used synthetic fabricated fractures and/or gas-water or oil-water as fluids. This experimental study will use a real fractured rock core from The Geysers geothermal field to study steam-water relative permeability.

Nitrogen and helium permeability experiments were conducted on the core to determine the effects of the rock fractures and to investigate the constraints and practicalities of conducting multiphase flow experiments in real geothermal rocks. The core contains several fractures as determined from an X-ray computer tomography image.

## 3.2 EXPERIMENTAL METHODOLOGY

The rock permeability was measured using nitrogen and helium gas at room temperature. Since gas permeability is a function of pressure, as described by Equation 3.1, the flow measurements were conducted at a series of different mean pressures.

$$k_{gas} = k_{abs}\left(1 - \frac{b}{p_{ave}}\right) \qquad (3.1)$$

The core sample was obtained from a depth of 1409.3m at The Geysers geothermal field. It is 4.70 cm in length and 6.91 cm in diameter.

At different confining pressures nitrogen was flowed into the core. Confining pressure from 500 to 850 psig was applied by injecting nitrogen around the heat shrink tubing inside the core holder. To apply a confining pressure of 1150 psig, water was used in place of nitrogen.

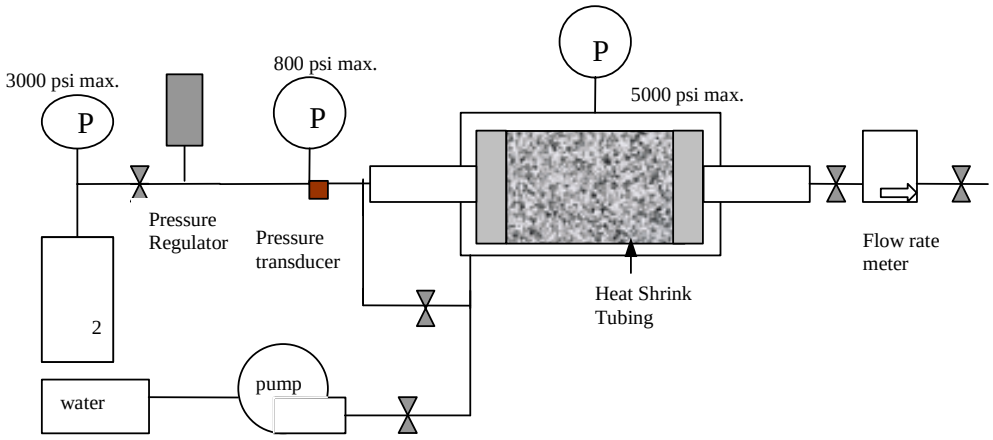


*Figure 3.1: Apparatus for flow measurement in geothermal rock.*

A pressure gauge and a pressure transducer connected to a digital display measured pressure at the inlet. The pressure at the outlet was taken to be 1 atm. The flow rate at the outlet was measured using a Matheson flow rate meter and controller (Model 8272-MF2000). The flow rate transducer calibration equation used was that determined by Kewen Li when he used the device in his experiments on slip factors (Oct-Dec 1999 Quarterly Report).

To determine the resistivity-saturation correlation for The Geysers core using two metal endplates, the apparatus shown below was used.

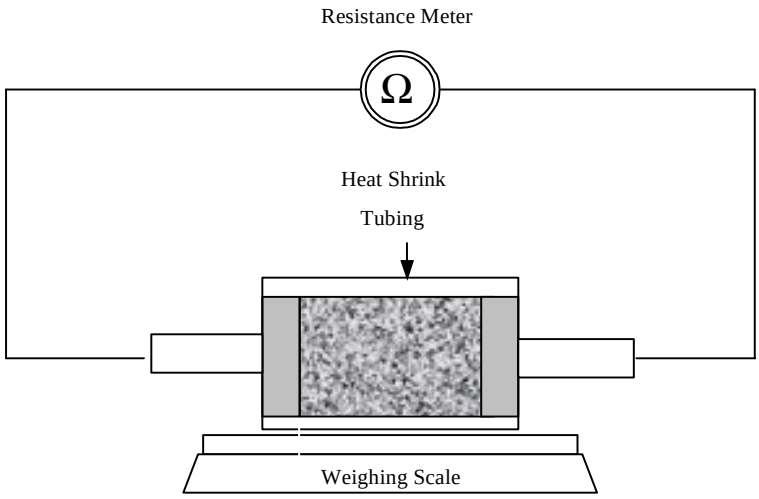


*Figure 3.2: Apparatus for determining resistivity-saturation correlation in geothermal rock.*

The core was saturated fully with water and then wrapped with heat shrink tubing, with the two metal plates attached on both ends of the core. The core was then allowed to dry on a weighing scale. Resistance measurements were measured for every 0.1 gram decrease in mass of the saturated core. Resistivity and resistivity indices were calculated for each resistance reading by using Equation 3.2 and 3.3.

$$\rho = r(\frac{A}{L}) \qquad (3.2)$$

$$R_{index} = \frac{\rho_{partiallysaturated}}{\rho_{fullysaturated}} \qquad (3.3)$$

where $r$ is resistance
$A$ is area
$L$ is length
ρ is resistivity

In preparation for conducting another nitrogen-water relative permeability experiment, a 2 inch diameter core was cut from The Geysers geothermal rock obtained at a depth of 1450 metres.

## 3.3 PARTIAL RESULTS AND DISCUSSION

Results of the nitrogen experiments are shown in Figure 3.3.

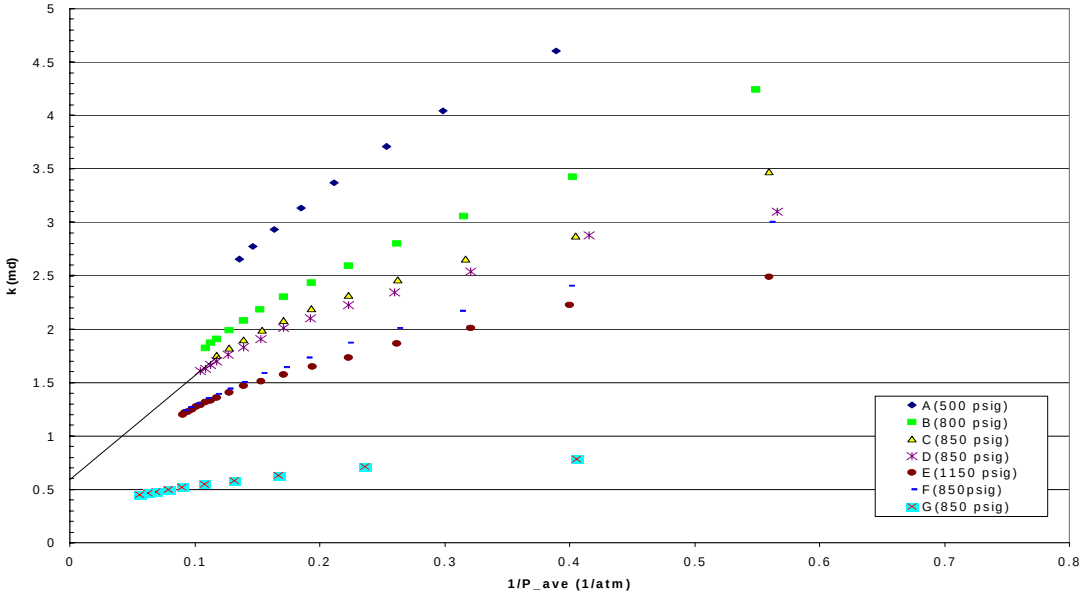


*Figure 3.3: Nitrogen permeability as a function of pressure.*

The intersection of the extrapolated lines with the vertical axis in the plot of permeability ($k$) versus the reciprocal of the mean pressure ($1/p_{ave}$) is taken to be the absolute permeability of the rock. At a confining pressure of 850 psig the absolute permeability is approximately 0.56 md. The permeability value labeled G was measured recently and differs from other permeability curves at 850 psig. This is due to the core being wet after the nitrogen-water relative permeability experiment.

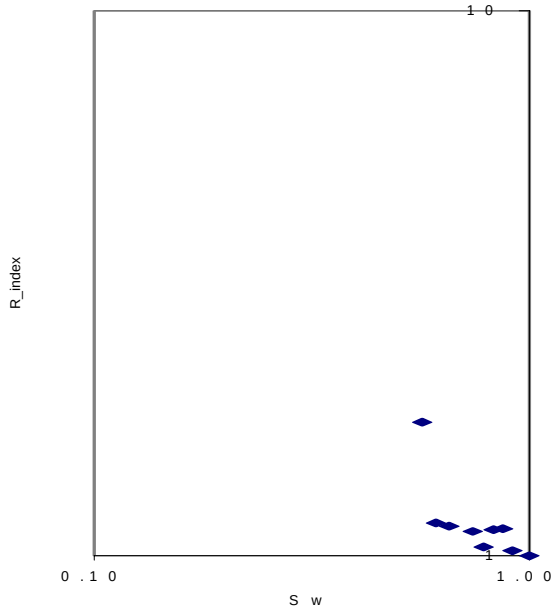


*Figure 3.4: Resistivity index vs. saturation for geothermal core.*

Results of the resistivity-saturation experiment are shown in Figure 3.4. A linear relationship is evident between the resistivity index and the water saturation in a log-log plot. The outlying point in the above figure occurs at 57% water saturation. Resistance measurements exceed the sensitivity of the resistance meter at water saturations below 57%.

To measure resistance at lower saturations, a variable resistor will be attached parallel to the core. Modeling of a variable resistance in parallel with the core is summarized in Figure 3.5.

The maximum resistance value that can be measured by the resistance meter is 40 megaohms. The optimal resistor value in parallel with the core is the maximum *R2* value that will result in a measured resistance, *R_total,* less than 40 megaohms. Choosing a lower value may increase errors in measurements because resistance readings, *R_total*, for different core resistance values may not be very different.

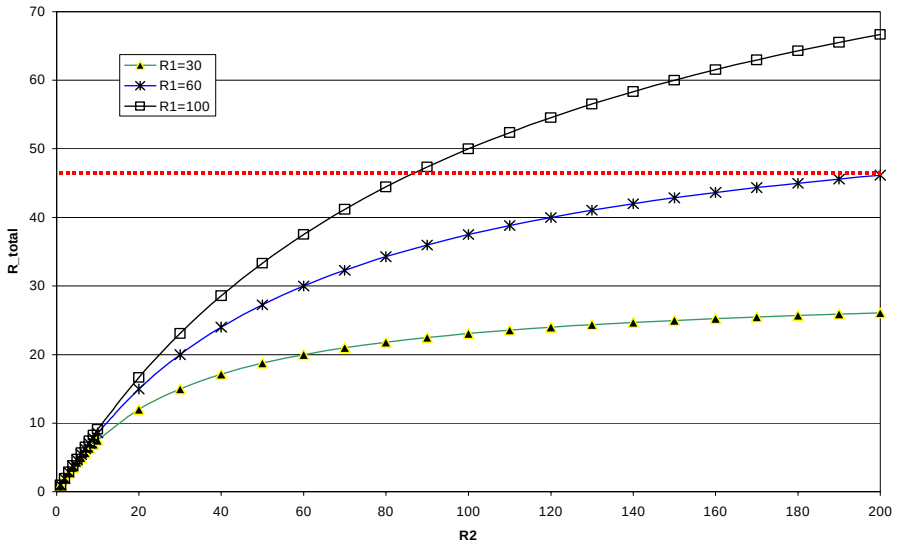


*Figure 3.5: R_total (measured resistance) vs. R2 (variable resistance) at different R1 (Saturated core resistance). All units in megaohms.*

## 3.4 CONTINUING AND FUTURE WORK

The next steps in the project will be as follows:

(1) Conduct resistivity-saturation experiments with a variable resistor in parallel with the core to be able to measure resistance values at lower saturations.

(2) Conduct nitrogen-water relative permeability experiments using the new 2 inch diameter core and new endplates with Torlon covered stems. Torlon is a stiff electrical insulator. Saturation will be measured in three ways:

(a) resistivity-saturation relationship

(b) weighing method

(c) mass balance

# 4. A GENERALIZED SCALING MODEL OF SPONTANEOUS IMBIBITION DATA

This research project was conducted by Research Associate Kewen Li and Professor Roland Horne. The goal of this study was to develop a generalized method to scale the experimental data of spontaneous water imbibition for any fluid-rock systems (gas-liquid-rock and liquid-liquid-rock systems). In this report, a general model was derived mathematically.

## 4.1 SUMMARY

We conducted a theoretical analysis and achieved a general method to scale the experimental data of spontaneous imbibition for any systems based on our previous method. We defined a dimensionless time with relative permeability, capillary pressure, wettability, and gravity included. The definition was not empirical but based on theoretical derivation. Relative permeability instead of absolute permeability was used in the dimensionless time. The new dimensionless time defined in this study could reduce to the existing definitions in specific cases in which relative permeability, capillary pressure, wettability, and gravity are not considered.

## 4.2 INTRODUCTION

An important fluid flow phenomenon during water injection or aquifer invasion into fractured reservoirs is spontaneous imbibition of the wetting phase. Scaling the experimental data of spontaneous imbibition in different fluid-rock systems is of essential importance to designing the water injection projects and predicting the reservoir production performances. Ignoring the effects of relative permeability, capillary pressure, wettability, and gravity in the dimensionless time might be the reason that the existing scaling methods do not always successfully function. It is known that these parameters significantly influence the fluid flow in porous media. Therefore these parameters should be included in the scaling model. Previously, we developed a method to scale the cocurrent spontaneous water imbibition into gas-saturated rocks (Li and Horne, 2002). The effects of relative permeability, capillary pressure, wettability, and gravity were considered in this method for gas-liquid-rock systems. However this method can not be applied to other systems, such as oil-water-rock systems, because the mobility of the nonwetting phase was assumed infinite. Therefore, a general method was developed to scale the experimental data of spontaneous imbibition for any systems such as oil-gas-rock, gas-water-rock, and oil-water-rock systems in both cocurrent and countercurrent spontaneous imbibition cases.

## 4.3 THEORY

Assuming Darcy's Law during the process of spontaneous imbibition that occurs vertically upward in a core with a specific value of initial saturation of the wetting phase ($S_{wi}$), including the zero $S_{wi}$, the volumetric fluxes of the wetting and the nonwetting phases in the core sample are expressed as follows:

$$v_w = -\frac{k_w}{\mu_w}\left(\frac{\partial p_w}{\partial x} + \rho_w g\right) \tag{4.1a}$$

$$v_{nw} = -\frac{k_{nw}}{\mu_{nw}}\left(\frac{\partial p_{nw}}{\partial x} + \rho_{nw} g\right) \tag{4.1b}$$

where $v_w$ and $v_{nw}$ are the volumetric fluxes of the wetting and nonwetting phases; $k_w$ and $k_{nw}$ are the effective permeabilities of the wetting and nonwetting phases; $\mu_w$ and $\mu_{nw}$ are the viscosities of the wetting and nonwetting phases; $\rho_w$ and $\rho_{nw}$ the densities of the wetting and nonwetting phases; $p_w$ and $p_{nw}$ are the pressures of the wetting and nonwetting phases at the position $x$. From the definition of capillary pressure, the pressure of the wetting phase can be calculated:

$$p_w = p_{nw} - P_c \tag{4.2}$$

where $P_c$ is the capillary pressure.

Substituting Eq. 4.2 into Eq. 4.1a:

$$v_w = M_w\left(\frac{\partial P_c}{\partial x} - \frac{\partial p_{nw}}{\partial x} - \rho_w g\right) \tag{4.3}$$

where

$$M_w = \frac{k_w}{\mu_w} \tag{4.4}$$

Eq. 4.1b could be written as follows:

$$\frac{\partial p_{nw}}{\partial x} = -\left(\frac{v_{nw}}{M_{nw}} + \rho_{nw} g\right) \tag{4.5}$$

where

$$M_{nw} = \frac{k_{nw}}{\mu_{nw}} \tag{4.6}$$

In cocurrent spontaneous imbibition flow, the following equation applies:

$$v_w = v_{nw} \tag{4.7}$$

In countercurrent spontaneous imbibition flow, the following equation applies:

$$v_w + v_{nw} = 0 \tag{4.8}$$

We first consider the cocurrent spontaneous imbibition. Because the flux of the nonwetting phase is equal to that of the wetting phase, Eq. 4.5 could be reduced:

$$\frac{\partial p_{nw}}{\partial x} = -(\frac{v_w}{M_{nw}} + \rho_{nw} g) \tag{4.9}$$

Substituting Eq. 4.9 into Eq. 4.3:

$$v_w = \frac{M_w M_{nw}}{M_{nw} - M_w}(\frac{\partial P_c}{\partial x} - \Delta\rho g) \tag{4.10}$$

where $\Delta\rho$ is the density difference between the wetting phase and the nonwetting phase ($=\rho_w - \rho_{nw}$).

We define that:

$$M_e = \frac{k_e}{\mu_e} = \frac{M_w M_{nw}}{M_{nw} - M_w} \tag{4.11}$$

where $M_e$ is a coefficient called the effective mobility, representing the combined effect of the mobilities of both the wetting and the nonwetting phases on the spontaneous imbibition. $k_e$ and $\mu_e$ are the effective permeability and the effective viscosity of the two phases respectively.

It is assumed in this study that the wetting phase imbibes into rocks in a piston-like manner. In such an imbibition flow, the following equation holds:

$$\frac{\partial P_c}{\partial x} = \frac{P_c}{x} \tag{4.12}$$

Substituting Eqs. 4.11 and 4.12 into Eq. 4.10:

$$v_w = M_e(\frac{P_c}{x} - \Delta\rho g) \tag{4.13}$$

Assuming that the distribution of $S_{wi}$ in the porous medium is homogeneous, the accumulated volume of the wetting phase imbibed into the core with $S_{wi}$ can be calculated as follows:

$$N_{wt} = Ax\phi(S_{wf} - S_{wi}) \tag{4.14}$$

where $N_{wt}$ is the accumulative volume of the wetting phase imbibed into the core and $A$ is the cross-section area of the core.

The imbibition rate of the wetting phase $Q_w$ is equal to $Av_w$ in cocurrent spontaneous imbibition. Therefore, Eq. 4.13 can be expressed as follows:

$$Q_w = AM_e(\frac{P_c}{x} - \Delta\rho g) \tag{4.15}$$

Substituting Eq. 4.14 into Eq. 4.15:

$$Q_w = a_0\frac{1}{R} - b_0 \tag{4.16}$$

where

$$a_0 = \frac{AM_e(S_{wf} - S_{wi})}{L}P_c \tag{4.17a}$$

$$b_0 = AM_e\Delta\rho g \tag{4.17b}$$

$$R = \frac{N_{wt}}{V_p} \tag{4.17c}$$

where $V_p$ is the pore volume of the core sample; $R$ is the recovery by spontaneous imbibition in terms of pore volume.

Define that:

$$c_0 = \frac{b_0}{a_0} \tag{4.18a}$$

$$R^* = c_0 R \tag{4.18b}$$

and

$$t_d = c_0^2 \frac{k_e}{\phi} \frac{P_c}{\mu_e} \frac{S_{wf} - S_{wi}}{L_a^2} t \tag{4.18c}$$

here $c_0$ is the ratio of the gravity force to the capillary force, $t_d$ is the dimensionless time with gravity and capillary forces included. $R^*$ is the normalized recovery. In the cocurrent spontaneous imbibition case, $L_a$ is equal to the core length.

Substituting Eqs. 4.18a, 4.18b, and 4.18c into Eq. 4.16, the following equation is obtained:

$$\frac{R^* dR^*}{dt_d} = 1 - R^* \tag{4.19}$$

In cases of $R^*$ less than 1.0, the solution of Eq. 4.19 is:

$$(1 - R^*) e^{R^*} = e^{-t_d} \tag{4.20}$$

We can see from Eq. 4.20 that $R^*$ is only a function of the newly defined dimensionless time. This feature shows that experimental data from spontaneous imbibition in rocks with different size, porosity, permeability, initial fluid saturation, interfacial tension, and wettability can be scaled to a single curve of $R^*$ vs. $t_d$.

For countercurrent spontaneous imbibition, the only difference is the expression of the effective mobility, which is represented as follows:

$$M_e = \frac{k_e}{\mu_e} = \frac{M_w M_{nw}}{M_{nw} + M_w} \tag{4.21}$$

The procedure to scale the spontaneous imbibition using the new method is described briefly in the following. The imbibition rate is first plotted vs. the reciprocal of the recovery (amount of the wetting phase imbibed into the core in terms of pore volume). A straight line is expected from which the values of the two constants $a_0$ and $b_0$ could be obtained from linear regression analysis. The effective mobility, $M_e$, and the capillary pressure, $P_c$, at $S_{wf}$ could also be calculated once the values of $a_0$ and $b_0$ are available. Therefore the dimensionless time defined in Eq. 4.18c and the normalized recovery defined in Eq. 4.18b could be computed. Finally, the normalized recovery is plotted vs. the new dimensionless time. According to Eq. 4.20, the experimental data of spontaneous imbibition in different rocks with different specific properties is expected to correlate in the form of the normalized recovery vs. the new dimensionless time.

In gas-liquid-rock systems, the mobility of the nonwetting phase (gas) is usually much greater than that of the wetting phase. Hence $M_e$ is closely equal to $M_w$. In this case, the general scaling model (Eqs. 4.18b and 4.18c) developed in this study could be reduced to the model that we previously developed (see Li and Horne, 2002). All the other equations are also the same as in gas-liquid-rock systems.

The general dimensionless time defined in Eq. 4.18c could also reduce to the definition by Zhou *et al*. (2001) if gravity is neglected and only interfacial tension instead of capillary pressure is considered.

## 4.4 DISCUSSION

A unique feature of the general scaling model developed in this study is the consideration of capillary pressure instead of only interfacial tension. This is important because interfacial tension only represents the fluid property while spontaneous imbibition is also governed significantly by fluid-rock and rock properties such as wettability and pore structure. Unlike interfacial tension, capillary pressure includes not only fluid-fluid property but also fluid-rock and rock properties.

## 4.5 CONCLUSIONS

Based on the present study, the following conclusions may be drawn:

1. A general scaling model was developed for any fluid-rock systems in both cocurrent and countercurrent spontaneous imbibition.
2. The general scaling model could reduce to the model that we previously developed for gas-liquid-rock systems and could also reduce to the model proposed by Zhou *et al*. (2001) if gravity is neglected and only interfacial tension instead of capillary pressure is considered.

## 4.6 FUTURE WORK

We will verify the general model developed in this study using experimental data of spontaneous imbibition in both gas-water-rock and oil-water-rock systems.

## 5. REFERENCES


Arps, J.J.: "Analysis of Decline Curves," *Trans*. AIME (Dec. 1945) 160, 228-247.

Chen, H.Y. and Teufel, L.W.: "A New Rate-Time Type Curve for Analysis of Tight-Gas Linear and Radial Flows," paper SPE 63094, presented at the 2000 SPE Annual Technical Conference and Exhibition, Dallas, TX, October 1-4, 2000.

Corey, A.T., "The Interrelations Between Gas and Oil Relative Permeabilities," *Producers Monthly* Vol. 19 (1954), pp 38-41.

Cuttler, W.W. Jr.: "Estimation of Underground Oil Reserves by Oil-Well Production Curves," *Bull*., USBM (1924) 228.

Diomampo, G., " Relative Permeability through Fracture", MS thesis, Stanford University, Stanford, California (2001).

Faulder, D.D.: "Advanced Decline Curve Analysis in Vapor-Dominated Geothermal Reservoirs," paper SPE 38763, presented at the 1997 SPE Annual Technical Conference and Exhibition, San Antonio, TX, October 5-8, 1997.

Fetkovich, M.J.: "Decline Curve Analysis Using Type Curves," *JPT* (June. 1980) 1065-1077.

Fourar, M. and Bories, S.,: "Experimental Study of Air-Water Two-Phase Flow Through A Fracture (Narrow Channel)," *Int. J. Multiphase Flow* Vol. 21, No. 4, Toulouse, France (1995) pp. 621-637.

Fourar, M., Bories., Lenormand, R., and Persoff, P.,: "Two-Phase Flow in Smooth and Rough Fractures: Measurement and Correlation by Porous-Medium and Pipe Flow Models," *Water Resources Research* Vol. 29 No. 11. November 1993, pp. 3699-3708.

Fraim, M.L. and Wattenbarger, R.A.: "Gas Reservoir Decline Analysis Using Type Curves With Real Gas Pseudopressure and Normalized Time," *SPEFE* (December 1987).

Horne, R.H., Satik, C., Mahiya, G., Li, K., Ambusso, W., Tovar, R., Wang, C., and Nassori, H.: "Steam-Water Relative Permeability," *Proc. of the World Geothermal Congress* 2000, Kyushu-Tohoku, Japan, May 28-June 10, 2000.

Kneafsy, T. J. and Pruess, K.,: "Laboratory Experiments on Heat-Driven Two-Phase Flows in Natural and Artificial Rock Fractures," *Water Resources Research* Vol. 34, No. 12, December 1998, pp. 3349-3367.

Li, K., and Horne, R.N., "Accurate Measurement of Steam Flow Properties," *GRC Transactions* 23 (1999).

Li, K. and Horne, R.N. (2001a): "Characterization of Spontaneous Water Imbibition into Gas-Saturated Rocks," *SPEJ* (December 2001), p62-69.

Li, K. and Horne, R. N. (2001b): Quarterly Report for June-September 2001, Stanford Geothermal Program, DE-FG07-95ID13763.

Li, K. and Horne, R.N.: "Scaling of Spontaneous Imbibition in Gas-Liquid Systems," SPE 75167, to be presented at the SPE/DOE Thirteenth Symposium on Improved Oil Recovery held in Tulsa, Oklahoma, April 13–17, 2002.

Lockhart, R. W. and Martinelli, R.C.,: "Proposed Correction of Data for Isothermal two-phase component flow in pipes," *Chem. Eng. Prog*., Vol. 45, No. 39, 1949.

Mahiya, G., "Experimental Measurement Of Steam-Water Relative Permeability," MS thesis, Stanford University, Stanford, California (1999).

Pan, X., Wong, R.C., and Maini, B.B.: Steady State Two-Phase Flow in a Smooth Parallel Fracture, presented at the 47th Annual Technical Meeting of the Petroleum Society in Calgary, Alberta, Canada, June 10-12, 1996.

Palacio, J.C. and Blasingame, T.A.: "Decline Curve Analysis Using Type Curves: Analysis of Gas Well Production Data," paper SPE 25909 presented at the 1993 SPE Rocky Mountain Regional/Low Permeability Reservoirs Symposium, Denver, CO, April 12-14.

Persoff, P. K., Pruess, K. and Myer, L.: "Two-Phase Flow Visualization and Relative Permeability Measurement in Transparent Replicas of Rough-Walled Rock Fractures," *Proc. 16th Workshop on Geothermal Reservoir Engineering*, Stanford University, Stanford, California, January 23-25, 1991

Persoff, P., and Pruess, K.: "Two-Phase Flow Visualization and Relative Permeability Measurement in Natural Rough-Walled Rock Fractures," *Water Resources Research* Vol. 31, No. 5, May, 1995, pp. 1175-1186.

Pruess, K., and Tsang, Y. W.: "On Two-Phase Relative Permeability and Capillary Pressure of Rough-Walled Rock Fractures," *Water Resources Research* Vol. 26 No. 9, September 1990, pp 1915-1926.

Rodriguez, F. and Cinco-Ley, H.: "A New Model for Production Decline," paper SPE 25480 presented at the Production Operations Symposium, Oklahoma City, OK, March 21-23, 1993.

Scheidegger, A.E. *The Physics of Flow Through Porous Media*, 3rd ed., University of Toronto, Toronto. 1974.

Su, G. W., Geller, J. T., Pruess, K. and Wen, F.,: "Experimental Studies of Water Seepage and Intermittent Flow in Unsaturated, Rough-Walled Fractures," *Water Resources Research*, Vol. 35, No. 4, April 1999, pp. 1019-1037.

Zhou, D., Jia, L., Kamath, J., and Kovscek, A. R.: "An Investigation of Counter-Current Imbibition Processes in Diatomite," paper SPE 68837, presented at the 2001 SPE Western Regional Meeting, Bakersfield, California, March 26-30, 2001.

Witherspoon, P.A., Wang, J.S.W., Iwai, K. and Gale, J.E.: " Validity of Cubic Law for Fluid Flow in a Deformable Rock Fracture," *Water Resources Research*, Vol. 16, No. 6, 1980, pp 1016-1024.